The Role of Chemistry in Graphene Doping for Carbon-Based Electronics

Razvan A. Nistor, Dennis M. Newns, and Glenn J. Martyna*

IBM Research Division, T. J. Watson Research Center, P.O. Box 218, Yorktown Heights, New York 10598, United States

ABSTRACT Graphene forms an important two-dimensional (2D) material class that displays both a high electronic conductivity and optical transparency when doped. Yet, the microscopic origin of the doping mechanism in single sheet or bulk intercalated systems remains unclear. Using large-scale *ab initio* simulations, we show the graphene surface acts as a catalytic reducing/oxidizing agent, driving the chemical disproportionation of adsorbed dopant layers into charge-transfer complexes which inject majority carriers into the 2D carbon lattice. As pertinent examples, we focus on the molecular $SbCl_5$ and HNO_3 intercalates, and the solid compound $AlCl_3$. Identifying the microscopic mechanism for the catalytic action of graphene is important, given the availability of large area graphene sheets, to spur research into new redox reactions for use in science and technology.

KEYWORDS: graphene · doping · *ab initio* simulations · redox reactions · catalysis

Graphene[1,2] is a novel zero band gap semiconductor with high carrier mobility,[3,4] high optical transparency,[5] and high tensile strength.[6] It is a truly two-dimensional (2D) material, composed of a single atomic layer of sp^2-bonded carbons (Figure 1a). To facilitate transport in graphene based devices, the carrier concentration of the carbon layer must be adjusted by shifting the Fermi level of graphene's unique zero-gap band structure away from the Dirac point where the density of states (DOS) is zero (Figure 1a).[7] The desired rigid band shift can be induced by electrostatic gating[1] or chemical doping.[8] The latter is employed to enhance graphene's conductive properties in applications such as transparent electrodes for solar cells, which ideally would be formed from two-dimensional metals.[9,10] In conventional (3D) semiconductors, doping is achieved by substituting charge-donating species into the solid matrix. The binding energy of the dopant Rydberg states is reduced by the square of the dielectric constant, thereby facilitating dopant ionization at room-temperature. Graphene's two-dimensional nature precludes this bulk mechanism.

Graphene can be doped through a variety of chemical means that preserve its sp^2 lattice structure. Both hole (*p*) or electron (*n*) doping can be achieved by contacting the carbon layer with different metals.[11,12] Graphene grown epitaxially on SiC is naturally *n*-doped,[13] yet injecting or removing carriers is possible by chemically treating the substrate or graphene surface itself.[14,15] When an individual sheet is placed on Si or SiO_2 substrates, dangling bonds at the surface or unintentional exposure to oxygen, moisture, or residuals from the transfer process can lead to doping.[16−19] Other elements (typically B or N) can be directly substituted into the carbon lattice during the growth of the layers donating or removing electrons from the delocalized p_z-band.[20−23] Alternatively graphene can be doped through controlled and scalable processes by the adsorption of chemical species on its surface.[24−32] This latter method is a convenient way to enhance the electrical properties of carbon-based electronics[8,33,34] and novel devices exploiting graphene's sensitivity to changes in its carrier concentration.[35,36] The doping process here is enabled by charge transfer induced disproportionation reactions.[37] We will use large-scale *ab initio* simulation studies to elucidate the new physics of this novel doping mechanism.

RESULTS AND DISCUSSION

For molecular adsorbates, we shall show that the disproportionation/doping reaction is initiated because graphene, functioning as a metal,[38−40] lowers the activation barrier for the disproportionation of the parent dopant compound. The chemical origin of the weakened bond is an initial, yet incomplete, charge transfer between the adsorbed species and the graphene lattice which acts to destabilize the chemical integrity of the parent compound. This destabilization facilitates the disproportionation reaction into open-shell chemical products that heavily dope the graphene by injecting majority carriers to the carbon lattice (Figure 1b).

* Address correspondence to martyna@us.ibm.com.

Received for review January 19, 2011 and accepted March 10, 2011.

Published online March 10, 2011
10.1021/nn200225f

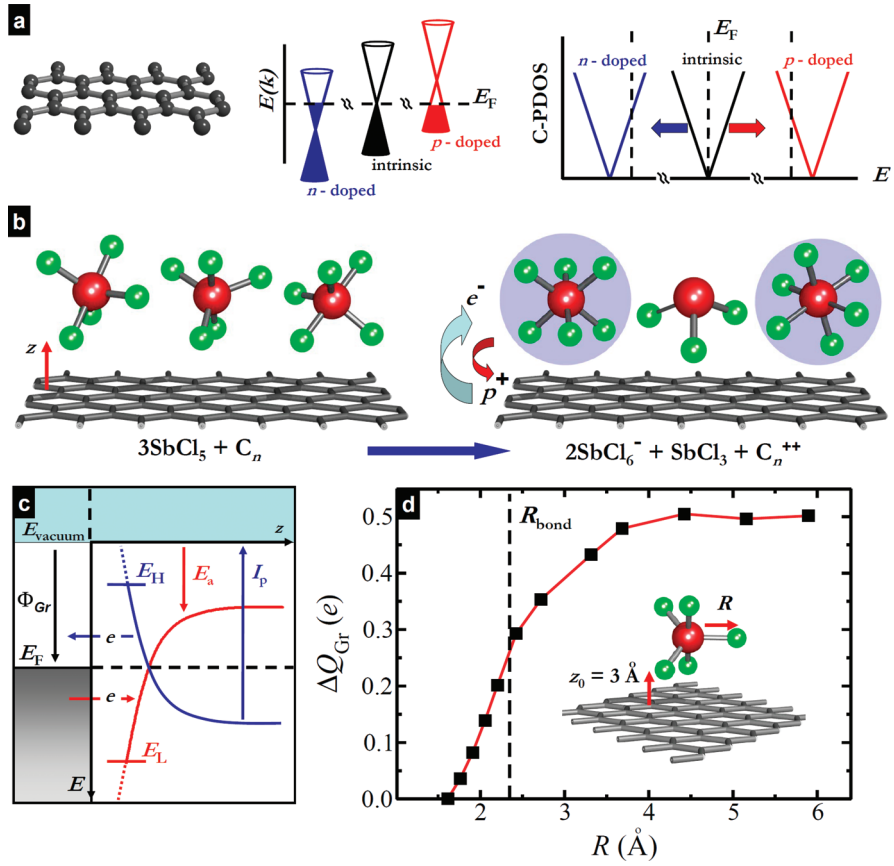

Figure 1. The doping mechanism in graphene: catalysis and disproportionation. (a) Atom-thick sp^2-bonded carbon lattice of graphene characterized by the linear $E(k)$ dispersion relation. Electrons (or holes) transferred to the carbon layer shift the Fermi level away from the Dirac point, shown as an energy shift in the carbon projected density of states (C-PDOS). (b) Closed-shell molecular dopant destabilized by partial carrier transfer with the graphene surface (shown for the *p*-doping $SbCl_5$ complex as an example: Sb, brown; Cl, green). The parent compound dissociates into open-shell products which absorb minority carriers from the graphene, highlighted in blue. (c) Graphene acting as a metal surface. Charge is transferred to (or from) the dopant species as its distance from the surface decreases, altering the position of its valence energy level relative to the graphene work function Φ_{Gr}. For *p*-dopants, the electron affinity E_a increases as electrons are added to the valence level (for *n*-dopants, the ionization potential I_p decreases as electrons are removed). Degree of charge transfer is defined by the final energetic alignment between Φ_{Gr} and the LUMO E_L (or HOMO E_H) level at equilibrium separation. (d) Charge transfer to the graphene ΔQ_{Gr} as a function of reaction coordinate. In this case, R, the bond length between a Cl and the Sb in an $SbCl_5$ molecule suspended at its equilibrium height (3 Å) above a graphene plane. The dashed line R_{bond} indicates the equilibrium bond length.

When a closed-shell *p*-dopant having a lowest unoccupied molecular orbital (LUMO), approaches the graphene surface (Figure 1c), the electron affinity level $E_a = E_{vacuum} - E_L$ is lowered by the image force $E_a \rightarrow E_a(z)$, which in linearized Thomas–Fermi approximation has the asymptotic form,

$$E_{im}(z) \approx E_a(\infty) - \frac{e^2}{4z} + \mathcal{O}(z^{-2}) \qquad (1)$$

where e is the elementary unit of charge and z is the height of the adsorbate above the graphene plane.[41,42] In the conventional Newns–Anderson model,[43−46] the lowering of the LUMO is also accompanied by a broadening due to the interaction with the low-lying energy bands of a transition metal substrate. This combined effect allows partial charge to transfer to the adsorbate as it approaches the surface.[38,44,45] Furthermore, in the chemisorbed limit, strong interactions with the narrow metal *d*-band lying close to the Fermi energy tend to cause splitting of the hybridized adsorbate–substrate levels into bonding and antibonding pairs.[44−47] Graphene lacks this narrow *d*-band feature and the foregoing partial filling of the of the adsorbate levels seems to provide an adequate description for the dopants that will be considered here. However, the formation of strong covalent bonds on the surface as in graphane[48] and graphene-oxide[49] shows that for small atoms at short bond lengths, a version of the Newns–Anderson model may be applicable.

For *n*-dopants with an highest occupied molecular orbital (HOMO), the hole-density has a similar but mirrored affect on the HOMO energy level, lowering the ionization potential I_p of the adsorbed species (Figure 1c). In this case, charge flows to the graphene from the dopant as the HOMO level nears the graphene Fermi energy. In the case of dopants such as

alkali metals, their ionization potential in monatomic form is already low enough for significant charge transfer to occur in the absence of any dissociative degree of freedom.

For molecular *p*-doping adsorbates, the initial charge transfer into the dopant LUMO level destabilizes the dopant compound driving the reaction coordinate toward disproportionation. We exemplify this in terms of a lengthening of a bond coordinate *R* leading to dissociation (Figure 1d); the charge transfer from graphene increases as the bond dissociates. Charge also flows *via* tunneling as the height of the dopant is varied from the surface (see the online Supporting Information). Upon dissociation, the LUMO is pushed far below the level of the graphene work function.[25] The degree of charge transfer from the carbon layer is governed by the final energetic alignment of the graphene work function and the dopant LUMO E_L level at equilibrium separation. Chemically, this transfer in surface-doped graphene systems is driven by an effective 2D surface-induced electronegativity equalization principle (2SEE). Graphene's unique electronic properties are sensitive to any subsequent changes in its carrier concentration, becoming more metallic with any rigid band shift to which the 2SEE mechanism naturally leads. That is, graphene functions as a novel 2D surface catalyst, facilitating the disproportionation of adsorbed dopant layers into charge transfer complexes which in turn strongly dope, but (ideally) have no other effect on the graphene.

Enhancing material properties through adsorption or by intercalation, that is, the insertion of chemical species into the lamellar matrix of layered compounds, was used as early as 700CE to augment the strength and transparency of Chinese porcelain.[50,51] Intercalates have since been employed to tailor the electronic properties of graphite, increasing the inplane conductivity of this semimetal to near copper values.[51−55] The intercalation process typically proceeds under harsh chemical conditions, high temperatures, and/or pressures. It is unclear whether edge interactions with the graphite material, the inordinate environment of the process, or the surface of the carbon layers drives the disproportionation reaction.[54] In contrast to graphite, graphene allows for assembly of intercalated systems in which experimental studies can be performed under mild conditions by stacking individually grown graphene sheets that have been immersed in a chemical bath of the intercalate species (typically strong Lewis acids). Such few-layered assemblies are required in transparent electrode applications. In the following, we use *ab initio* simulations to track the emerging open-shell molecular complexes for two molecular based *p*-doping intercalates, $SbCl_5$ and HNO_3, on graphene. We demonstrate the spontaneous disproportionation of the bulk parent compounds when they are placed between graphene bilayers following the mechanism described above. We also investigate the disproportionation reaction involving the solid compound $AlCl_3$.

A common graphitic intercalate used recently as a dopant in carbon-based electronics is composed of antimony−chloride molecular complexes.[33,56] The parent compound of this intercalate is the strong Lewis acid $SbCl_5$. In graphite, the fluidlike intercalate layer is composed of a mixture of open- and closed-shell antimony species including $SbCl_3$, $SbCl_4$, and $SbCl_6$.[57] Antimony can accommodate such diverse bonding configurations because of its ability to form sp^3d^n hybridized orbitals, where $n = 0,1,2$. We track in a clean fashion the emergence of open-shell entities by performing a 30 ps room temperature simulation of an $SbCl_5$:C_{14} bilayer system (see the Supporting Information video 1). We observe the spontaneous transfer of a chlorine atom from one $SbCl_5$ unit to another under the catalytic action of the carbon sheet. The graphene induced disproportionation of $SbCl_5$ is observed to follow the reaction known to occur in bulk graphite,[54]

$$6SbCl_5 + C_{84} \rightarrow C_{84}^{2+}(2SbCl_6^-) + SbCl_3 + 3SbCl_5 \quad \textbf{(2)}$$

In Figure 2, we quantify the degree of charge transfer from the graphene lattice as the disproportionation reaction proceeds. A snapshot of an undissociated sample (Figure 2a) shows in its corresponding projected density of states PDOS (Figure 2b) that the parent $SbCl_5$ compound absorbs only a small fraction of charge from the graphene layer. As the reaction progresses, the chlorine atoms, destabilized by this initial transfer of electron density, form a chlorine bridge between two $SbCl_5$ entities (Figure 2c), increasing carrier injection to the graphene (Figure 2d). Stable $SbCl_6$ complexes are formed after the simulation equilibrates (Figure 2e). The electronic structure of the resulting dissociated intercalate layer (Figure 2f) has the usual features of strong graphene *p*-doping:[25] the LUMO of antimony-chlorides at the Fermi level of the system is 0.8 eV below the Dirac point of graphene, facilitating the electron transfer from the carbon lattice.

The progressive degree of *p*-doping of the carbon lattice by the initial undissociated molecular layer ($\Delta Q_{Gr} = +0.2e$/84C), through to the bridged structure ($\Delta Q_{Gr} = +0.5e$/84C), and onto the final dissociated products ($\Delta Q_{Gr} = +1.6e$/84C) as shown in Figure 2a−f, is in line with the 2SEE principle: Carrier transfer to the graphene increases as the parent compound dissociates and the valence band of the dopant falls progressively below the Dirac point of the graphene. The $SbCl_5$ system exhibits spontaneous charge-induced disproportionation driven by the 2SEE principle, resulting in significant doping of the graphene. Our results demonstrate the dynamic nature of this intercalate layer as (energetically favorable) open-shell molecular species form on the graphene surface. Also of note,

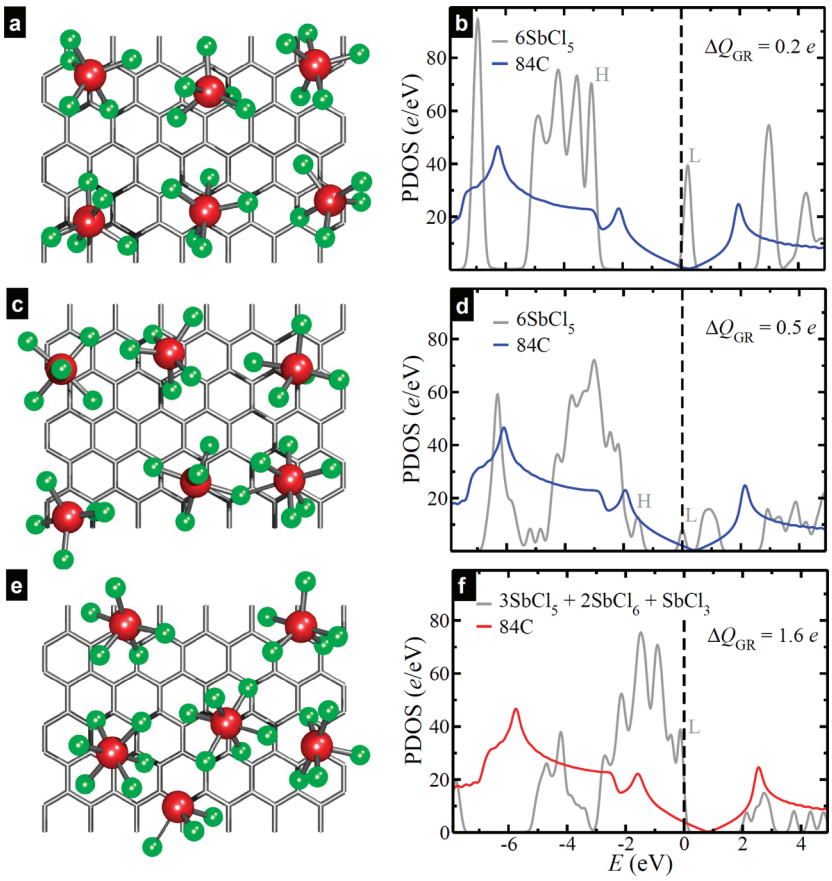

Figure 2. Graphene driven dissociation of adsorbed $SbCl_5$. (a) Undissociated $SbCl_5$ complexes in a graphene bilayer (top carbon layer not shown): Sb, brown; Cl, green; graphene, wire mesh. (b) Projected density of states (PDOS) of panel a showing unperturbed but slightly doped (+0.2*e* charge on graphene) carbon PDOS and the HOMO (H) and LUMO (L) positions of the dopant layer. LUMO level aligned near Dirac point at Fermi energy. (c) Chlorine bridge forms spontaneously between two $SbCl_5$ complexes after 8 ps of simulation; intermittent step in formation of stable open-shell complexes. (d) PDOS of panel c showing increased +0.5*e* charge transfer from graphene. LUMO level lies 0.5 eV below Dirac point. (e) Equilibrated configuration showing stable open-shell complexes $SbCl_6$ have formed *via* the disproportionation reaction given in text. (f) PDOS of panel e showing maximal charge transfer from graphene +1.6*e* due to low lying LUMO level 0.8 eV below Dirac point.

open-shell products of the $SbCl_5$ intercalate do not form in a cluster-phase (graphene-free) simulation of comparable duration.

Nitric acid (HNO_3) is another example of a classic *graphitic* hole-donor that has recently been used to dope graphene for photovoltaic applications.[34] To study this system, we equilibrate a sample of nitric acid molecules placed in a graphene bilayer at the frequently cited experimental density of HNO_3:C_5.[54,58,59] In an undissociated configuration, the HNO_3 molecules form an incommensurate hydrogen bonded network between the graphene sheets (Figure 3a and the X-ray diffraction data in Figure 3b). The corresponding electronic structure analysis (Figure 3c) shows that only a slight charge transfer from the carbon layer occurs for this sample. All molecular orbitals of the intercalate molecules are completely filled, the highest band of which (HOMO) lies 2.3 eV below the Fermi level, and 2.5 eV below the Dirac point within the local spin density approximation (LSDA). The LUMO is concomitant with the Dirac point, and hence, in an energetically unfavorable position to accept carriers from the carbon lattice.

The direct energetic barrier for the dissociation of nitric acid along the HO−NO_2 path is high, 3.5 eV within LSDA compared to the experimental 3.2 eV,[60] and is reduced (quite significantly) by the presence of the graphene sheet (2.5 eV). Yet, to drive the spontaneous disproportionation of this *p*-dopant during the time scales available in our simulations, we either alter the initial torsional angle of each HNO_3 molecule (+0.4 eV/molecule), or add a single oxygen molecule to the initial intercalate layer (see the online Supporting Information video files 2 and 3). The resulting analyses of the products produced by the two initial conditions both generate the NO_3^- moiety responsible for strongly doping the graphene. Equilibration of the former initial condition leads to the 2SEE driven disproportionation of the system (Figure 3d) given by

$$10HNO_3 + 50C \rightarrow (6HNO_3)2NO_3^- C_{50}^+ + 2NO_2 + 2H_2O \quad (3)$$

which is in line with experimentally reported bulk graphite reaction,[54,58] and X-ray diffraction data

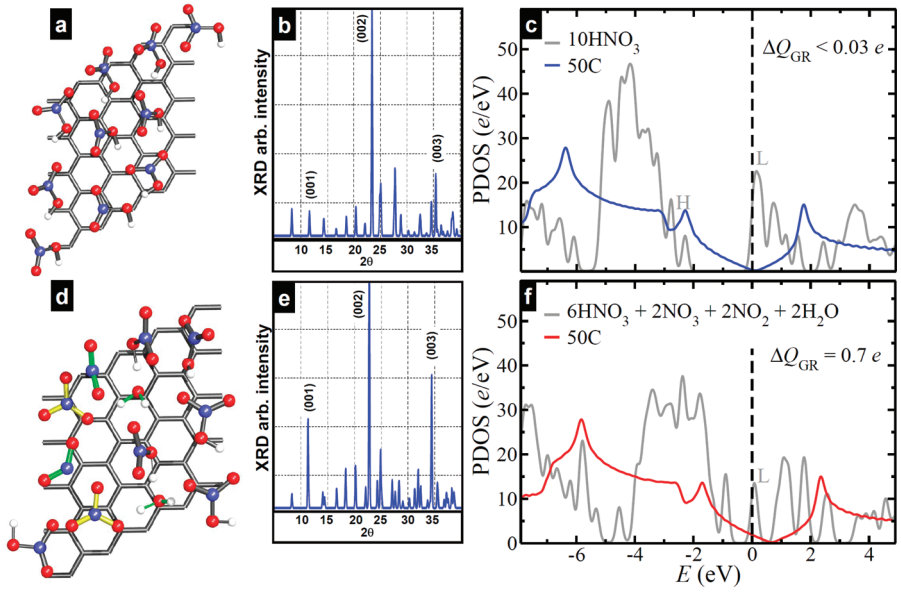

Figure 3. Dissociation of nitric acid on graphene. (a) Undissociated configuration of hydrogen bonded HNO_3 network in a graphene bilayer (top carbon layer not shown): N, blue; O, red; H, white; graphene, wire mesh. (b) Bulk XRD spectra of configuration shown in panel a. (c) PDOS of panel a showing alignment of LUMO (L) level of HNO_3 layer and graphene Dirac point with little charge transfer from the carbon layer. (d) Dissociated HNO_3 configuration with strongly doping NO_3^- moiety (bonds colored yellow). Also present are NO_2^- and H_2O complexes (bonds colored green). (e) Bulk XRD spectra of dissociated HNO_3 layer shown in panel d with prominent (002) peak at $2\theta = 22.5$ and showing enhanced (001) peak at $2\theta = 11.3$ in agreement with experimental data. (f) PDOS of panel d showing large charge transfer to carbon layer $+0.7e$. LUMO of dissociated HNO_3 layer lies 0.6 eV below Dirac point.

(compare Figure 3e with Figure 3b); a strong (002) peak appears at $2\theta = 22.5$, and the (001) peak at 11.3 is enhanced.[59] The position of the Dirac point of the carbon PDOS (Figure 3f) is shifted to higher energy relative to the Fermi level of the system, indicative of *p*-doping. The LUMO of the intercalate layer lies 0.7 eV below the Dirac point, allowing for significant transfer from the graphene sheet, but only following the dissociation of the parent compound.

As a final example of a 2SEE driven disproportionation on graphene, we investigate the doping mechanism of a common nonmolecular salt, $AlCl_3$.[52,62] A single layer of the $AlCl_3$ crystal can be lattice-matched to a graphene cell with a resultant density of $Al:C_{6.25}$ (see the online Supporting Information). Upon thermalization, the $AlCl_3$ compound retains its stable bulk crystal structure (see Figure 4a and the X-ray diffraction data in Figure 4b). The resulting electronic structure analysis (Figure 4c) shows no charge transfer to the graphene layer occurs, the LUMO of the salt lying a full 2 eV above the Dirac point. Significant doping of the graphene layers in this material can only be achieved by reducing the aluminum concentration of the initial compound,[53] essentially creating aluminum vacancies between the graphene layers. The excess chlorine allows the strong doping $AlCl_4^-$ moiety to be formed within the solid intercalate layer. The aluminum depletion realizes the disproportionation reaction involving the crystal, graphene, and residual chlorine gas of the environment in which intercalates are synthesized experimentally.[52,54]

We can construct such an aluminum depleted configuration from a reaction of the form,

$$4(Al_2Cl_6)_g + 3(Cl_2)_g + C_{50} \rightarrow [(8Al_{0.75}Cl_3)^-_{ads}C^+_{50}] + (Al_2Cl_6)_g \quad (4)$$

the quantity in square brackets representing the adsorbed (ads) configuration of interest (Figure 4d). Following this reaction, the dopant density becomes $Al:C_{8.33}$, a best match to the experimentally reported $Al:C_{7.5}$[61] or $Al:C_{10}$,[53] given the limitations of the simulation system size. Such aluminum depletion of the intercalate compound is in agreement with experimental X-ray diffraction data; the height of the (003) peak increasing relative to the (002) peak (compare Figure 4b and 4e).[54,61,63] The resulting electronic structure analysis of the aluminum-depleted configuration (Figure 4f) shows a significant charge transfer from the graphene layer occurs, the LUMO of the salt lying 1.0 eV below the Dirac point.

Simulations of intercalated graphene systems have demonstrated that the graphene surface acts as a generalized reducing agent, driving the disproportionation of closed-shell parent intercalated compounds into charge-transfer complexes which thereby dope the carbon lattice. The disproportionation reaction is initiated by an image-force lowering of the molecular affinity level (see eq 1) allowing charge to more easily flow from the carbon layer. For the molecular intercalates examined ($SbCl_5$ and HNO_3), the graphene sheets function as charge reservoirs, donating

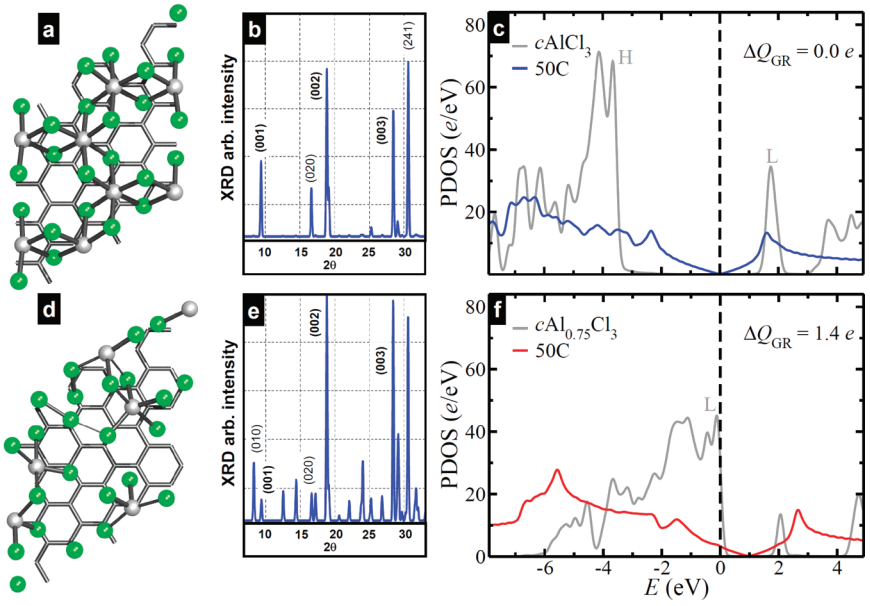

Figure 4. $AlCl_3$ doping of graphene. (a) Lattice matched $cAlCl_3$ single layer in graphene bilayer (top carbon sheet not shown): Al, gray; Cl, green; graphene, wire mesh. (b) Bulk XRD spectrum of configuration shown in panel a displaying higher intensity (002) peak at $2\theta = 18.5$ compared to (003) peak at $2\theta = 28.5$. (c) PDOS of $AlCl_3$ salt showing no doping of graphene as LUMO (L) level lies 2 eV above Dirac point. (d) Aluminum deficient configuration $cAl_{0.75}Cl_3$. (e) Bulk XRD spectrum of configuration shown in panel d with more prominent (003) peak, in line with experimental trend. (d) PDOS of panel d showing large charge transfer to the graphene sheet +1.4*e* as the LUMO of the aluminum depleted salt lies 1.0 eV below the Dirac point.

electrons to the adsorbed species, destabilizing their bonds, and lowering the activation barriers for dissociation. No intermediate functionalization involving the graphene is necessary for the reaction to proceed. Rather, graphene's role as a metallic surface (albeit, a two-dimensional one) facilitates disproportionation and charge transfer as shown in Figure 1b. For the salt ($AlCl_3$), we find a cation deficiency is necessary for doping, which is typically achieved experimentally by forming the intercalate in an atmosphere rich in the molecular form of the anion (Cl_2); this chemistry is simply another disproportionation reaction. Understanding the microscopic origin of the catalytic action of graphene and wide availability of large sheets of graphene[64] allows the possibility for a new set of catalytic reactions with important applications in biology, chemistry as well as engineering and technology.

METHODS

The simulations presented herein were performed with Car–Parrinello *ab initio* molecular dynamics (CPMD)[65] using a plane-wave representation of the Kohn–Sham orbitals in the density functional theory (DFT).[66,67] DFT is currently the most tractable way of solving the time-independent Schrödinger equation for large systems, reducing a 3*n* many body problem (3 spatial degrees of freedom given *n* electrons) to just the 3 spatial degrees of freedom of the electron density. For dynamics, the electronic states and classical nuclear coordinates were propagated within the canonical ensemble using a time step of 0.0625 fs and Nosé-Hoover chain thermostats[68] to ensure a constant temperature of 300 K. The dynamics simulations were performed using the OpenAtom software package[69] on 2048 nodes of IBM's T. J. Watson BlueGene/L supercomputer. The Perdew–Zunger local density approximation (PZ-LDA)[70] was used to model electronic exchange and correlation effects since it gives artificially stronger binding between molecular entities and the graphene surface compared to generalized gradient approximation (GGA) functionals. The pseudopotentials used in the dynamics were of the Martin–Troulliers type.[71] Simulations were performed with a minimum cutoff energy of 30 Ry at the Γ point. Electronic structure calculations were performed with the Quantum Espresso software package[72] on relaxed configurations obtained from the dynamics results. A plane-wave energy cutoff of 60 Ry (816 eV) and $9 \times 9 \times 1$ k-point grids were used for the initial self-consistent calculations. The density of states (DOS) were calculated with $15 \times 15 \times 1$ dense k-point grids. Ultrasoft pseudopotentials[73] were used when possible except for antimony (Sb) and chlorine (Cl) which were of the norm conserving Bachelet–Hamann–Schlüter type.[74] Both LDA and GGA functionals yielded similar DOS results.

Acknowledgment. Funding support from the IBM Research Division and the Egypt Nanotechnology Center (EGNC) is gratefully acknowledged. The authors wish to thank P. Avouris, J. Tersoff, M. A. Kuroda, and A. A. Maarouf for useful discussions.

Supporting Information Available: Videos 1–3 as explained in the text; further information regarding the methods used in this paper, as well as additional analyses of the systems in Figures 2–4. This material is available free of charge *via* the Internet at http://pubs.acs.org.

REFERENCES AND NOTES

1. Novoselov, K. S.; Geim, A. K.; Morozov, S. V.; Jiang, D.; Zhang, Y.; Dubonos, S. V.; Grigorieva, I. V.; Firsov, A. A. Electric Field Effect in Atomically Thin Carbon Films. *Science* **2004,** *306*, 666–669.

2. Berger, C.; Song, Z.; Li, T.; Li, X.; Ogbazghi, A. Y.; Feng, R.; Dai, Z.; Marchenkov, A. N.; Conrad, E. H.; First, P. N.; *et al*. Ultrathin Epitaxial Graphite: 2D Electron Gas Properties and a Route Toward Graphene-Based Nanoelectronics. *J. Phys. Chem. B* **2004,** *108*, 19912–19916.
3. Novoselov, K. S.; Geim, A. K.; Morozov, S. V.; Jiang, D.; Katsnelson, M. I.; Grigorieva, I. V.; Dubonos, S. V.; Firsov, A. A. Two-Dimensional Gas of Massless Dirac Fermions in Graphene. *Nature* **2005,** *438*, 197–200.
4. Bolotin, K. I.; Sikes, K. J.; Jiang, Z.; Klima, M.; Fudenberg, G.; Hone, J.; Kim, P.; Stormer, H. L. Ultrahigh Electron Mobility in Suspended Graphene. *Solid State Commun.* **2005,** *146*, 351–355.
5. Nair, R. R.; Blake, P.; Grigorenko, A. N.; Novoselov, K. S.; Booth, T. J.; Stauber, T.; Peres, N. M. R.; Geim, A. K. Fine Structure Constant Defines Visual Transparency of Graphene. *Science* **2008,** *320*, 1308.
6. Lee, C.; Wei, X.; Kysar, J. W.; Hone, J. Measurement of the Elastic Properties and Intrinsic Strength of Monolayer Graphene. *Science* **2008,** *321*, 385–388.
7. Geim, A. K.; Novoselov, K. S. The Rise of Graphene. *Nat. Mater.* **2007,** *6*, 183–191.
8. Avouris, P.; Chen, Z; Perebeinos, V. Carbon-Based Electronics. *Nat. Nanotechnol.* **2007,** *2*, 605–615.
9. Wang, X.; Zhi, L.; Müllen, K. Transparent, Condutive Graphene Electrodes for Dye-Sensitized Solar Cells. *Nano Lett.* **2008,** *8*, 323–327.
10. Kim, Ke. S.; Zhao, Y.; Jang, H.; Lee, S. Y.; Kim, J. M.; Kim, Kw. S.; Ahn, J.-H.; Kim, P.; Choi, J.-Y.; Hong, B. H. Large-Scale Pattern Growth of Graphene Films for Stretchable Transparent Electrodes. *Nature* **2009,** *457*, 706–710.
11. Giovannetti, G.; Khomyakov, P. A.; Brocks, G.; Karpan, V. M.; van den Brink, J.; Kelly, P. J. Doping Graphene with Metal Contacts. *Phys. Rev. Lett.* **2008,** *101*, 026803-1–026803-4.
12. Khomyakov, P. A.; Starikov, A. A.; Brocks, G.; Kelly, P. J. Nonlinear Screening of Charges Induced in Graphene by Metal Contacts. *Phys. Rev. B* **2010,** *82*, 115437-1–115437-6.
13. Chen, W.; Chen, S.; Qi, D. C.; Gao, X. Y.; Wee, A. T. S. Surface Transfer p-Type Doping of Epitaxial Graphene. *J. Am. Chem. Soc.* **2007,** *129*, 10418–10422.
14. Coletti, C.; Riedl, C.; Lee, D. S.; Krauss, B.; Patthey, L.; von Klitzing, K.; Smet, J. H.; Starke, U. Charge Neutrality and Band-Gap Tuning of Epitaxial Graphene on SiC by Molecular Doping. *Phys. Rev. B* **2010,** *81*, 235401-1–235401-8.
15. Choi, J.; Lee, H.; Kim, K.-J.; Kim, B.; Kim, S. Chemical Doping of Epitaxial Graphene by Organic Free Radicals. *J. Phys. Chem. Lett.* **2010,** *1*, 505–509.
16. Stampfer, C.; Molitor, F.; Graf, D.; Ensslin, K.; Jungen, A.; Hierold, C.; Wirtz, L. Raman Imaging of Doping Domains in Graphene on SiO_2. *Appl. Phys. Lett.* **2007,** *91*, 241907-1–241907-3.
17. Casiraghi, C.; Pisana, S.; Novoselov, K. S.; Geim, A. K.; Ferrari, A. C. Raman Fingerprint of Charged Impurities in Graphene. *Appl. Phys. Lett.* **2007,** *91*, 233108-1–233108-3.
18. Kang, Y.-J.; Kang, J; Chang, K. J. Electronic Structure of Graphene and Doping Effect on SiO_2. *Phys. Rev. B* **2008,** *78*, 115404-1–115404-5.
19. Ryu, S.; Liu, L.; Berciaud, S.; Yu, Y.-J.; Liu, H.; Kim, P.; Flynn, G. W.; Brus, L. E. Atmospheric Oxygen Binding and Hole Doping in Deformed Graphene on a SiO_2 Substrate. *Nano Lett.* **2010,** *10*, 4944–4951.
20. Wang, X.; Li, X.; Zhang, L.; Yoon, Y.; Weber, P. K.; Wang, H.; Guo, J.; Dai, H. *n*-Doping of Graphene Through Electrothermal Reactions with Ammonia. *Science* **2009,** *324*, 768–771.
21. Wei, D.; Liu, Y.; Wang, Y.; Zhang, H.; Huang, L.; Yu, G. Synthesis of *n*-Doped Graphene by Chemical Vapor Deposition and Its Electrical Properties. *Nano Lett.* **2009,** *9*, 1752–1758.
22. Panchakarla, L. S.; Subrahmanyam, K. S.; Saha, S. K.; Govindaraj, A.; Krishnamurthy, H. R.; Waghmare, U. V.; Rao, C. N. R. Synthesis, Structure, and Properties of Boron- and Nitrogen-Doped Graphene. *Adv. Mater.* **2009,** *21*, 4726–4730.
23. Guo, B.; Liu, Q.; Chen, E.; Zhu, H.; Fang, L.; Gong, J. R. Controllable *n*-Doping of Graphene. *Nano Lett.* **2010,** *10*, 4975–4980.
24. Schedin, F.; Geim, A. K.; Morozov, S. V.; Hill, E. W.; Blake, P.; Katsnelson, M. I.; Novoselov, K. S. Detection of Individual Gas Molecules Adsorbed on Graphene. *Nat. Mater.* **2007,** *6*, 652–655.
25. Wehling, T. O.; Novoselov, K. S.; Morozov, S. V.; Vdovin, E. E.; Katsnelson, M. I.; Geim, A. K.; Lichtenstein, A. I. Molecular Doping of Graphene. *Nano Lett.* **2008,** *8*, 173–177.
26. Leenaerts, O.; Partoens, B; Peeters, F. M. Adsorption of H_2O, NH_3, CO, NO_2, and NO on Graphene: A First-Principles Study. *Phys. Rev. B* **2008,** *77*, 125416-1–125416-6.
27. Gierz, I.; Riedl, C.; Starke, U.; Ast, C. R.; Kern, K. Atomic Hole Doping of Graphene. *Nano Lett.* **2008,** *8*, 4603–4607.
28. Kim, K. K.; Reina, A.; Shi, Y.; Park, H.; Li, L.-J.; Lee, Y. H.; Kong, J. Enhancing the Conductivity of Transparent Graphene Films *via* Doping. *Nanotechnology* **2010,** *21*, 285205-1–285205-6.
29. Liu, L.; Ryu, S.; Tomasik, M. R.; Stolyarova, E.; Jung, N.; Hybertsen, M. S.; Steigerwald, M. L.; Brus, L. E.; Flynn, G. W. Graphene Oxidation: Thickness-Dependent Etching and Strong Chemical Doping. *Nano Lett.* **2008,** *8*, 1965–1970.
30. Farmer, D. B.; Golizadeh-Mojarad, R.; Perebeinos, V.; Lin, Y.-M.; Tulevski, G. S.; Tsang, J. C.; Avouris, P. Chemical Doping and Electron-Hole Conduction Asymmetry in Graphene Devices. *Nano Lett.* **2009,** *9*, 388–392.
31. Dong, X.; Fu, D.; Fang, W.; Shi, Y.; Chen, P.; Li, L.-J. Doping Single-Layer Graphene with Aromatic Molecules. *Small* **2009,** *5*, 1422–1426.
32. Chen, J.-H.; Jang, C.; Adam, S.; Fuhrer, M. S.; Williams, E. D.; Ishigami, M. Charged-Impurity Scattering in Graphene. *Nat. Phys.* **2008,** *4*, 377–381.
33. Chen, J.; Klinke, C.; Afzali, A; Avouris, P. Self-Aligned Carbon Nanotube Transistors with Charge Transfer Doping. *Appl. Phys. Lett.* **2005,** *86*, 123108-1–123108-3.
34. Kasry, A.; Kuroda, M. A.; Martyna, G. J.; Tulevski, G. S; Bol, A. A. Chemical Doping of Large-Area Stacked Graphene Films for Use as Transparent, Conducting Electrodes. *ACS Nano* **2010,** *4*, 3839–3844.
35. Qu, L.; Liu, Y.; Baek, J.-B.; Dai, L. Nitrogen-Doped Graphene as Efficient Metal-free Electrocatalyst for Oxygen Reduction in Fuel Cells. *ACS Nano* **2010,** *4*, 1321–1326.
36. Wang, Y.; Shao, Y.; Matson, D. W.; Li, J.; Lin, Y. Nitrogen-Doped Graphene and Its Application in Electrochemical Biosensing. *ACS Nano* **2010,** *4*, 1790–1798.
37. Selig, H.; Ebert, L. Graphite Intercalation Compounds. *Adv. Inorg. Chem. Radiochem.* **1980,** *23*, 281–327.
38. Gurney, R. W. Theory of Electrical Double Layers in Adsorbed Films. *Phys. Rev.* **1935,** *47*, 479–482.
39. Langmuir, I. Vapor Pressures, Evaporation, Condensation, and Adsorption. *J. Am. Chem. Soc.* **1932,** *54*, 2798–2832.
40. Neaton, J. B.; Hybertsen, M. S.; Louie, S. G. Renormalization of Molecular Electronic Levels at Metal−Molecule Interfaces. *Phys. Rev. Lett.* **2006,** *97*, 216405-1–216405-4.
41. Polini, M.; Tomadin, A.; Asgari, R; MacDonald, A. H. Density Functional Theory of Graphene Sheets. *Phys. Rev. B* **2008,** *78*, 115426-1–115426-12.
42. Ghaznavi, M.; Mišković, Z. L.; Goodman, F. O. Nonlinear Screening of External Charge by Doped Graphene. *Phys. Rev. B* **2010,** *81*, 085416-1–085416-12.
43. Anderson, P. W. Localized Magnetic States in Metals. *Phys. Rev.* **1961,** *124*, 41–53.
44. Newns, D. M. Self-Consistent Model of Hydrogen Chemisorption. *Phys. Rev.* **1969,** *178*, 1123–1135.
45. Hewson, A. C.; Newns, D. M. Effect of the Image Force in Chemisorption. *Jpn. J. Appl. Phys. Suppl.* **1974,** *2*, 121.
46. Chorkendorff, I.; Niemantsverdriet, J. W. In *Concepts of Modern Catalysis and Kinetics*; Wiley-VCH: Weinheim, Germany, 2003; pp 236−246.
47. Hammer, B.; Norskov, J. K. Why Gold Is the Noblest of All the Metals. *Nature* **1995,** *376*, 238–240.
48. Sofo, J. O.; Chaudhari, A. S.; Barber, G. D. Graphane: A Two-Dimensional Hydrocarbon. *Phys. Rev. B* **2007,** *75*, 153401-1–153401-4.

49. Dreyer, D. R.; Park, S.; Bielawski, C. W.; Ruoff, R. S. The Chemistry of Graphene Oxide. *Chem. Soc. Rev.* **2010,** *39*, 228–230.
50. Weiss, A. A Secret of Chinese Porcelain Manufacture. *Angew. Chem., Int. Ed.* **1963,** *2*, 697–703.
51. Ebert, L. B. Intercalation Compounds of Graphite. *Annu. Rev. Mater. Sci.* **1976,** *6*, 181–212.
52. Dresselhaus, M. S.; Dresselhaus, G Intercalation Compounds of Graphite. *Adv. Phys.* **2002,** *51*, 1–186.
53. Forsman, W. C.; Dziemianowicz, T.; Leong, K; Carl, D. Graphite Intercalation Chemistry: An Interpretive Review. *Synth. Met.* **1983,** *5*, 77–100.
54. McKelvy, M. J.; Glaunsinger, W. S. Molecular Intercalation Reactions in Lamellar Compounds. *Annu. Rev. Phys. Chem.* **1990,** *41*, 497–523.
55. Sorokina, N. E.; Nikol'skaya, I. V.; Ionov, S. G.; Avdeev, V. V. Acceptor-Type Graphite Intercalation Compounds and New Carbon Materials Based on Them. *Russ. Chem. Bull., Int. Ed.* **2005,** *54*, 1749–1767.
56. Chandra, B; Afzali, A.; Khare, N.; El-Ashry, M. M.; Tulevski, G. S. Stable Charge-Transfer Doping of Transparent Single Walled Carbon Nanotube Films. *Chem. Mater.* **2010,** *22*, 5179–5183.
57. Suzuki, M.; Suzuki, I. S.; Lee, C.; Niver, R.; Matsubara, K.; Sugihara, K. *c*-Axis Resistivity of $SbCl_5$ Graphite Intercalation Compounds. *J. Phys.: Condens. Matter.* **1997,** *9*, 10399–10420.
58. Fillaux, F.; Menu, S.; Conrad, J.; Fuzellier, H.; Parker, S. W.; Hanon, A. C.; Tomkinson, J. Inelastic Neutron Scattering Study of the Proton Dynamics in HNO_3 Graphite Intercalation Compounds. *Chem. Phys.* **1999,** *242*, 273–281.
59. Sorokina, N. E.; Maksimov, N. V; Avdeev, A. A. Anodic Oxidation of Graphite in 10 to 98% HNO_3. *Inorg. Mater.* **2001,** *37*, 360–365.
60. Johnstone, R. A. W.; Loureiro, R. M. S.; Cristiano, M. L. S.; Labat, G. Bond Energy/Bond Order Relationships for N-O Linkages and a Quantitative Measure of Ionicity: The Role of Nitro Groups in Hydrogen-Bonding. *ARKIVOC* **2010,** *2010*, 142–169.
61. Chien, T. R.; Marchesan, D.; Ummat, P. K.; Datars, W. R. The de Haas−van Alphen Effect of the Stage-1 $AlCl_3$ Graphite Intercalation Compound. *J. Phys.: Condens. Matter.* **1994,** *6*, 3031–3038.
62. Leung, S. Y.; Dresselhaus, M. S.; Underhill, C.; Krapchev, T.; Dresselhaus, G; Wuensch, B. J. Structural Studies of Graphite Intercalation Compounds Using (00*l*) X-ray Diffraction. *Phys. Rev. B* **1981,** *24*, 3505–3518.
63. Gualberto, G. M.; Underhill, C.; Leung, S. Y.; Dresselhaus, G. Raman and Infrared Spectra of Graphite-$AlCl_3$. *Phys. Rev. B* **1980,** *21*, 862–868.
64. Li, X.; Cai, W.; An, J.; Kim, S.; Nah, J.; Yang, D.; Piner, R.; Velamakanni, A.; Jung, I.; Tutuc, E.; *et al.* Large-Area Synthesis of High-Quality and Uniform Graphene Films on Copper Foils. *Science* **2009,** *324*, 1312–1314.
65. Car, R.; Parrinello, M. Unified Approach for Molecular Dynamics and Density Functional Theory. *Phys. Rev. Lett.* **1985,** *55*, 2471–2474.
66. Hohenberg, P.; Kohn, W. Inhomogeneous Electron Gas. *Phys. Rev.* **1964,** *136*, B864–B871.
67. Kohn, W.; Sham, L. J. Self-Consistent Equations Including Exchange and Correlation Effects. *Phys. Rev.* **1965,** *140*, A1133–A1138.
68. Martyna, G. J.; Klein, M. L.; Tuckerman, M. Nosé Hoover Chains: The Canonical Ensemble *via* Continuous Dynamics. *J. Chem. Phys.* **1992,** *97*, 2635–2644.
69. Bohm, E.; Bhatele, A.; Kale, L. V.; Tuckerman, M. E.; Kumar, S.; Gunnels, J. A.; Martyna, G. J. Fine-Grained Parallelization of the Car−Parrinello *ab Initio* Molecular Dynamics Method on the IBM Blue Gene/L Supercomputer. *IBM J. Res. Dev.* **2008,** *52*, 159–175.
70. Perdew, J. P.; Zunger, A. Self-Interaction Correction to Density-Functional Approximations for Many-Electron Systems. *Phys. Rev. B* **1981,** *23*, 5048–5079.
71. Troullier, N.; Martins, J. L. Efficient Pseudopotentials for Plane-Wave Calculations. *Phys. Rev. B* **1991,** *43*, 1993–2006.
72. Giannozzi, P.; Baroni, S.; Bonini, N.; Calandra, M.; Car, R.; Cavazzoni, C.; Ceresoli, D.; Chiarotti, G. L.; Cococcioni, M.; Dabo, I.; *et al.* QUANTUM ESPRESSO: A Modular and Open-Source Software Project for Quantum Simulations of Materials. *J. Phys.: Condens. Matter.* **2009,** *21*, 395502-1–395502-19.
73. Vanderbilt, D. Soft Self-Consistent Potentials in a Generalized Eigenvalue Formalism. *Phys. Rev. B* **1990,** *41*, 7892–7895.
74. Bachelet, G. B.; Hamann, D. R.; Schlüter, M. Pseudopotentials That Work: From H to Pu. *Phys. Rev. B* **1982,** *26*, 4199–4228.